NASA Contractor Report 189047

Prediction of Noise Field of a Propfan at Angle of Attack

Edmane Envia
Sverdrup Technology, Inc.
Lewis Research Center Group
Brook Park, Ohio

October 1991

Prepared for
Lewis Research Center
Under Contract NAS3-25266

National Aeronautics and
Space Administration

Prediction of Noise Field of a Propfan at Angle of Attack

Edmane Envia
Sverdrup Technology, Inc.
Lewis Research Center Group
Brook Park, Ohio 44142

ABSTRACT A method for predicting the noise field of a propfan operating at angle of attack to the oncoming flow is presented. The method takes advantage of the high-blade-count of the advanced propeller designs to provide an accurate and efficient formula for predicting their noise field. The formula, which is written in terms of the Airy function and its derivative, provides a very attractive alternative to the use of numerical integration. A preliminary comparison shows rather favorable agreement between the predictions from the present method and the experimental data.

1.1 Introduction

The need to limit both in-flight cabin noise and community noise has prompted the development of methods for accurate prediction of acoustic performance of propfans. A particular aim of these methods has been the prediction of the noise field of a propfan operating at angle of attack to the oncoming flow. Experimental evidence [1] suggest that the noise radiation characteristics of a propfan at angle of attack are significantly different from those of a propfan at zero angle of attack. These differences stem from the changes which occur both in the aerodynamics and aeroacoustics of a propeller whose axis is inclined with respect to the direction of oncoming flow.

One of the most important of these changes is the azimuthal variation of aerodynamic loading experienced by a propeller at angle of attack. Measurements [2], as well as numerical simulations [3], have shown that the loading variation or "unsteadiness" can be quite substantial over one period of revolution. Physically, the modulation occurs because propeller blades experience periodic variations in the local flow incidence. Acoustically, the loading unsteadiness creates a noise field which is axially non-symmetric. Methods which predict this effect have been in use for some time (see Hanson [4], for example).

Another feature of a propeller operating at angle of attack, which is ab-

sent at zero angle of attack case, is the cross-flow convective phase effect. This effect, first pointed out by Mani [5], may be explained as follows. For an inclined propeller, the oncoming flow has a nonzero velocity component in the plane of rotation. As a result, an acoustic source point fixed to the surface of the propeller "sees" a medium whose convective velocity varies periodically. This means that the convective phase of the sound radiated from this point is also periodically modulated. Krejsa [6], recently developed a prediction scheme which accounts for this effect by assuming that propeller sources are acoustically compact in the chordwise direction.

In this paper, a method which incorporates both the loading unsteadiness and cross-flow phase effects in a straightforward manner, without the simplifying assumptions such as chordwise compactness, is presented. This method, which is based on a moving-medium variant of the Ffowcs Williams and Hawkings [7] equation, relies on a frequency-domain formulation similar to that employed by Hawkings and Lawson [8] or Hanson [9], however, it differs from them in that the resulting Fourier integrals are evaluated asymptotically in the "large-blade-count limit" rather than in the far- or near-field limits. The advantage of this approach lies in the fact that it provides a uniform representation for the sound field in both the near- and far-fields while, at the same time, it affords the flexibility of using realistic blade geometries and aerodynamic loading distributions without their associated computational penalties.

1.2 Analysis

The starting point for the analysis is the moving-medium solution of the Ffowcs Williams and Hawkings equation for the acoustic pressure, $p(\mathbf{x},t)$, as given by Goldstein [10];

$$p(\mathbf{x},t) = -\int_{-\infty}^{+\infty}\int_{S(\tau)} \rho_0 v_n \frac{D_0 G}{D\tau}\, ds(\mathbf{y})\, d\tau + \int_{-\infty}^{+\infty}\int_{S(\tau)} f n_i \frac{\partial G}{\partial y_i}\, ds(\mathbf{y})\, d\tau + \int_{-\infty}^{+\infty}\int_{V(\tau)} T_{ij}\, \frac{\partial^2 G}{\partial y_i \partial y_j}\, d\mathbf{y}\, d\tau, \qquad (1a)$$

$$\frac{D_0}{D\tau} = \frac{\partial}{\partial \tau} + U_{0i}\, \frac{\partial}{\partial y_i}, \qquad (1b)$$

where ρ_0 is the ambient density, v_n the normal component of the surface relative velocity, f the amplitude of the aerodynamic loading, and T_{ij} the Lighthill stress tensor. $S(\tau)$ and $V(\tau)$ represent the propeller blade surfaces and the volume surrounding the blades, respectively. n_i's are components of the outward unit normal to S. It should be noted that the convention for the direction of the unit normal is opposite that of Goldstein's. The medium

convection velocity is denoted by U_0. $\mathbf{y}$ and $\mathbf{x}$ are the source and observer coordinates, respectively. τ denotes the source time and t the observer (i.e., retarded) time. The three terms in Eq. (1a) represent contributions from the thickness (monopole), loading (dipole) and stress (quadrupole) sources of noise. In this paper, however, the contribution from the last term will be ignored. The extension of the analysis to include quadrupole sources will be discussed elsewhere.

$G = G(\mathbf{x}, t/\mathbf{y}, \tau)$ in Eq. (1a) denotes the free-space moving-medium Green's function which may be written in the following form;

$$G = \frac{1}{4\pi\kappa R}\,\delta\left(t - \tau - g_c R/C_0\right), \tag{2a}$$

$$g_c(\tau) = \frac{1}{\beta_0^2}\left(\kappa - M_{0_R}\right), \qquad \kappa(\tau) = \left(M_{0_R}^2 + \beta_0^2\right)^{1/2},$$

$$M_{0_R}(\tau) = M_{0i}\, e_i, \qquad e_i(\tau) = \frac{(x_i - y_i)}{R}, \qquad \beta_0^2 = 1 - M_{0i}^2,$$

$$M_{0i} = \frac{U_{0i}}{C_0}, \qquad R(\tau) = |\mathbf{x} - \mathbf{y}(\tau)|. \tag{2b}$$

Here M_{0_R} is the component of the medium convection Mach number in the radiation direction, e_i's the components of the unit vector in the radiation direction, R the length of the radiation vector, and C_0 the medium speed of sound. Parameters g_c and κ represent the effects of medium convection on the retarded time and the spherical spreading rate, respectively. The explicit dependence of various parameters on the source time, τ, is indicated where necessary.

In order to simplify the description of the source motion, the 1-axis is chosen to coincide with the propeller shaft (see Fig. (1)). As a result the motion of the sources is confined to the transverse planes described by the 2– and 3–axes. In this coordinate system, the medium convection Mach number can be written as:

$$M_{01} = M_0 \cos\alpha, \qquad M_{02} = 0, \qquad M_{03} = M_0 \sin\alpha, \tag{3}$$

where α is the propeller angle of attack with respect to the oncoming flow as shown in Fig. (1).

Given the blade geometry and aerodynamic loading, the acoustic pressure, $p(\mathbf{x}, t)$, may be computed from Eq. (1a) for any observer location. This, of course, is the so called time-domain approach (see Farassat [11], for example) which entails solving transcendental equations for the source time, τ. Alternatively, one could use a frequency-domain approach which involves expanding the pressure field, $p(\mathbf{x}, t)$, in terms of its complex Fourier harmonic components, $p_k(\mathbf{x})$, i.e.,

$$p(\mathbf{x},t) = \sum_{k=-\infty}^{+\infty} p_k(\mathbf{x})\, e^{-ik\Omega t}, \tag{4a}$$

with the individual harmonic components given by:

$$p_k(\mathbf{x}) = \frac{\Omega}{2\pi}\int_0^{2\pi/\Omega} e^{ik\Omega t}\left[\int_{-\infty}^{+\infty}\int_{S(\tau)} \rho_0 v_n \frac{D_0 G}{Dt}\, ds(\mathbf{y})\, d\tau\right] dt -$$

$$\frac{\Omega}{2\pi}\int_0^{2\pi/\Omega} e^{ik\Omega t}\left[\int_{-\infty}^{+\infty}\int_{S(\tau)} f n_i \frac{\partial G}{\partial x_i}\, ds(\mathbf{y})\, d\tau\right] dt, \tag{4b}$$

where Ω is the propeller angular speed. In writing Eq. (4b), the derivatives of G with respect to the source coordinates from Eq. (1a) have been replaced by its derivatives with respect to the observer coordinates through the use of the simple relations:

$$\frac{\partial G}{\partial y_i} = -\frac{\partial G}{\partial x_i}, \qquad \frac{D_0 G}{D\tau} = -\frac{D_0 G}{Dt}. \tag{5}$$

Using the usual phase relationship arguments it can be shown that for B identical blades only p_k's for which $k = mB$ (where m is an integer) contribute to the infinite sum in Eq. (4a). This contribution is simply B times the contribution of a single blade. Therefore, from here on B will explicitly appear in the expressions for p_{mB} and, correspondingly, S will denote the surface of a single blade.

To further simplify Eq. (4b), the spatial derivatives, $\partial/\partial x_i$, of G may be rewritten in terms of the temporal derivative, $\partial/\partial t$, through the use of the chain rule;

$$\frac{\partial G}{\partial x_i} = -\left[\frac{1}{C_0}\frac{\partial (g_c R)}{\partial x_i}\frac{\partial}{\partial t} + \frac{1}{R}\frac{\partial R}{\partial x_i} + \frac{1}{\kappa}\frac{\partial \kappa}{\partial x_i}\right] G. \tag{6}$$

The temporal derivatives can now be removed using integration by parts and the integral over t, which involves a delta function, can then be easily evaluated to yield,

$$p_{mB}(\mathbf{x}) = \int_0^{2\pi/\Omega}\left[\int_{S(\tau)} Q_{\text{monopole}}(\mathbf{x},\mathbf{y},\tau)\, e^{imB\Omega(\tau + g_c R/C_0)}\, ds(\mathbf{y})\, d\tau\right] +$$

$$\int_0^{2\pi/\Omega}\left[\int_{S(\tau)} Q_{\text{dipole}}(\mathbf{x},\mathbf{y},\tau)\, e^{imB\Omega(\tau + g_c R/C_0)}\, ds(\mathbf{y})\, d\tau\right], \tag{7}$$

where Q_{monopole} and Q_{dipole} represent the expressions for the "amplitudes" of the two acoustic source. Note that the limits on the integration over τ

have been changed to reflect the fact that an interval of size $2\pi/\Omega$ in t is mapped exactly into an interval of size $2\pi/\Omega$ in τ. The expressions for the monopole and dipole source amplitudes are given by:

$$Q_{\text{monopole}} = -\frac{B\Omega\rho_0 v_n(\tau)}{8\pi^2}\left[\frac{imB\Omega}{\kappa R} - \frac{M_{0_i}}{\kappa^2 R}(e_i - g_c M_{0_i}) + \frac{M_{0_i}}{\kappa^3 R^2}\left(M_{0_R}\, M_{0_i} + \beta_0^2 e_i\right)\right], \quad (8a)$$

$$Q_{\text{dipole}} = \frac{B\Omega f(\tau)}{8\pi^2}\left[-\frac{imB\Omega n_i}{\kappa^2 R}(e_i - g_c M_{0_i}) + \frac{n_i}{\kappa^3 R^2}\left(M_{0_R}\, M_{0_i} + \beta_0^2 e_i\right)\right]. \quad (8b)$$

Note that, for a propeller operating at an angle of attack, v_n and f depend on τ. n_i and e_i also depend on τ even if the propeller is operating at zero angle of attack. Note also that, the definition of the source amplitude here differs from the standard one in that it includes the fall-off with distance R.

Once source amplitude distributions Q_{monopole} and Q_{dipole} are estimated, it remains to carry out the integrations in Eq. (7). Ordinarily, in the context of a frequency-domain analysis, the integral over τ is computed first. Since, for general geometries and source amplitudes, this integral is not tractable analytically, it is usually computed asymptotically for, say, near- or far-field observer locations for which the integrand may be simplified significantly. The result is given in terms of the appropriate Bessel functions. The remaining surface integral is then carried out analytically or numerically depending on how faithfully the blade geometry is to be represented.

There is, however, a less restrictive, and at the same time, more accurate way of computing $p_{mB}(\mathbf{x})$. This is accomplished by evaluating the τ integral asymptotically for large-blade-count, B (or more precisely mB), using a modification to the standard steepest descent and saddle point methods. The advantage of this approach lies in the fact that it does not require a near- or far-field approximation and, therefore, is applicable to general geometries and source amplitudes. The details of the derivation will be presented for the zero angle of attack case first. The results will then be used to derive an extension to the angle of attack cases most often encountered in practice. For the sake of brevity, the formula will be given in terms of a generic source amplitude Q. The resulting expression is therefore applicable to both the monopole and dipole sources.

1.2.1 Zero Angle of Attack Case ($\alpha = 0$)

Since, it is desirable to represent the blade geometry as accurately as possible, the surface integrals cannot be carried out analytically and must, instead, be performed using a suitable quadrature scheme. For practical considerations, it is more convenient to evaluate the surface integral first. To do so, we begin by dividing the blade surface into N_p small panels. If the typical panel size is sufficiently small the integrand may be assumed to be constant over the panel and, thus, the surface integral may be approximated by some appropriate "mean value" of the integrand times the panel surface area ΔS. If the mean value is chosen to be the value of the integrand at the geometric center of the panel, designated $\mathbf{y_S}$, the error in this approximation is $O(L^2)$ for a given N_p, where $L = |\mathbf{y} - \mathbf{y_S}|_{\max}$. Of course, the error could be made arbitrarily small by choosing a large enough N_p. Therefore, $P_{mB}(\mathbf{x})$ may be written as:

$$p_{mB}(\mathbf{x}) \simeq \sum_{n_p=1}^{N_p} \Delta S_{n_p}\, e^{-imB\Psi_c}\, I_{n_p}, \tag{9a}$$

$$I_{n_p} = \int_0^{2\pi} Q(\theta)\, e^{mB\Phi(\theta)}\, d\theta, \tag{9b}$$

$$\Phi(\theta) = i\left(\theta + a\sqrt{1 - b\cos\theta}\right), \tag{9c}$$

$$a = \frac{M_{tip}}{\beta_{0_1}\sqrt{\chi^2 + r^2 + r_s^2}}, \qquad b = \frac{2rr_s}{\chi^2 + r^2 + r_s^2}, \tag{9d}$$

$$\Psi_C = \frac{M_{tip} M_{0_1} \chi}{\beta_{0_1}} + \phi_s - \phi,$$

$$\chi^2 = \frac{1}{\beta_{0_1}^2}(x_1 - y_{s_1})^2, \qquad \beta_{0_1}^2 = 1 - M_{0_1}^2, \tag{9e}$$

where for brevity (x_1, x_2, x_3) and $(y_{s_1}, y_{s_2}, y_{s_3})$ have been replaced by their cylindrical polar counterparts (x_1, r, ϕ) and (y_{s_1}, r_s, ϕ_s), respectively. Furthermore, the integration variable τ is replaced by a new variable $\theta = \Omega\tau + \phi_s - \phi$. M_{tip} is the tip rotational Mach number (i.e., $R_{tip}\Omega/C_0$), ΔS_{n_p} the surface area of the n_pth panel and Ψ_C is a convective phase factor representing the collection of phase terms which do not depend on τ. $Q(\theta)$ is the source amplitude function written in terms of the variable θ. In order to simplify the notation, the explicit dependence of various variables on $\mathbf{y_S}$, the centroid of the n_pth panel, is suppressed. $\Phi(\theta)$ is the canonical phase function for a propeller operating at zero angle of attack, with a and b representing a combination of geometric, convective and kinematic factors. In deriving the above expressions, both the observer and source spatial coordinates are non-dimensionalized with respect to the propeller tip radius R_{tip}. (Note that, $M_{01} = M_0$ for zero angle of attack case.)

For a typical propfan $B = 8$, thus, even at the blade-passing-frequency (BPF), i.e., $m = 1$, the integrand in Eq. (9b) is highly oscillatory. Of course, one way to tackle the problem is to integrate the θ-integral using a suitable quadrature scheme. That was indeed the approach taken in Nallasamy et al. [12]. Unfortunately, accurate computation of higher harmonics (i.e., $m \geq 2$) requires an ever increasing quadrature resolution to capture the oscillatory nature of the integrand, and that may prove to be computationally expensive. It turns out, however, that it is possible to evaluate the integral I_{n_p} rather accurately using the steepest descent and saddle point methods. Naturally, in that case, the variable θ must be allowed to be complex and the integration path (i.e., $[0, 2\pi]$) be deformed into an appropriate contour.

Since in most practical applications of interest, propfans operate at a supersonic relative tip Mach number (i.e., $M_{(rel)tip} = (M_{tip}^2 + M_{01}^2)^{1/2}$), in the subsequent analysis it is assumed that $M_{(rel)tip} > 1$. Replacing θ with the variable, $\nu = \theta + i\sigma$, leads to a phase function, $\Phi(\nu)$, which is now also complex. It is fairly straightforward to find the saddle points of $\Phi(\nu)$ (i.e., $\Phi^{'}(\nu) = 0$, where $(')$ denotes differentiation with respect to ν) and the appropriate steepest descent contours. The easiest way to find the saddle points is to define an auxiliary variable $\xi = \cos\nu$, and rewrite $\Phi^{'}(\nu) = 0$ in terms of ξ;

$$(ab/2)^2\,\xi^2 \; - b\xi + 1 - (ab/2)^2 = 0, \tag{10}$$

where a and b were defined in Eq. (9d). Eq. (10) is clearly quadratic in ξ and may readily be solved. Thus, for given observer and source locations, $\Phi(\nu)$ has, in general, two simple saddle points in the interval $[0, 2\pi]$ which depending on whether the component of the source relative Mach number in the direction of the observer, i.e., $M_{(rel)_i}e_i$, is subsonic or supersonic, have different forms. The two are a complex conjugate pair if $M_{(rel)_i}e_i < 1$, and are real if $M_{(rel)_i}e_i > 1$. When $M_{(rel)_i}e_i = 1$ (i.e., the "sonic condition"), these two saddle points merge to give rise to a single second order saddle point. For a subsonic source, it turns out, that only one of the two saddle points lies on the appropriate steepest descent path and, hence, only that saddle point contributes to the integral. It should be noted that, the integrand also has an infinite number of branch points, coinciding with those of $\Phi(\nu)$, of which only four lie in the region of interest. A judicious choice of the branch cuts guarantees that the contributions to the contour integral along the cuts in the ν-plane is exponentially small compared with the contributions from the neighborhood of the saddle points. The location of the appropriate saddle points, branch cuts and steepest descent contours for typical source locations are shown in Fig. (2). Note that, the choice of the steepest descent path depends on the type of the source under consideration. Also shown in this Figure, are the auxiliary (descent) contours needed for deforming the original contour, $[0, 2\pi]$, into the steepest descent contour(s). Due to the periodicity of the integrand in θ, the contributions

from these contours cancel each other out exactly.

Naturally, the asymptotic structure of I_{n_p} for a sonic source point is different from that for a non-sonic one. In fact, it is fairly easy to show that the asymptotic expansion is given in terms of the inverse fractional 1/3-powers of parameter mB for sonic sources, and in terms of the inverse fractional 1/2-powers of mB for non-sonic sources. Since, there is no simple way of constructing a composite expansion from these two expansions, to allow for a smooth transition through the sonic condition, they are not very convenient to use. Fortunately, employing a theorem due to Chester, Friedman and Ursell [13], it is possible to develop a uniform expansion. The details of the method may be found in Bleistein and Handelsman [14] among others. The basic idea is, however, rather simple. The phase function $\Phi(\nu)$ is mapped conformally ($\nu \rightarrow \zeta$) into a much simpler function (i.e., a cubic polynomial in this case) which displays the relevant features of the original phase function. The region of interest in the complex ν-plane (i.e., the region containing the saddle points and steepest descent contours) is correspondingly mapped into a region in the complex ζ-plane. With the introduction of a few necessary parameters, the standard steepest descent and saddle point methods could then be applied to develop the required uniform expansion. The key definitions and parameters along with the final result are summarized below.

The cubic is given by:

$$\Phi(\nu) = -\left(\frac{\zeta^3}{3} - \gamma^2\zeta\right) + \mu, \tag{11a}$$

$$\mu = \frac{1}{2}\left[\Phi(\nu^+) + \Phi(\nu^-)\right], \qquad \gamma^3 = \frac{3}{4}\left[\Phi(\nu^+) - \Phi(\nu^-)\right], \tag{11b}$$

where ν^+ and ν^- denote the locations of the saddle points of Φ in the complex ν-plane and μ and γ are parameters defining the conformal map. Note that, γ, as given above, can take on three possible values or branches. The aforementioned theorem guarantees that one of the branches defines the desired conformal map (see Ref. [14] for details). That branch turns out to be the one for which γ^2 is purely real for the problem at hand. With these parameters determined, the map may be constructed and the uniform asymptotic expansion carried out. In principle, the expansion of the integral I_{n_p} could be carried out to an arbitrary order in the parameter mB, however, it turns out that, for most applications, the first term provides a very reasonable approximation for even the BPF component (i.e., $m = 1$). Therefore, in the subsequent analysis only the first term is considered.

After a fair amount of algebra, the final result can be written as the following formula:

$$I_{n_p} \simeq 2\pi i e^{mB\mu}\left\{d_0\frac{A_i[(mB)^{2/3}\gamma^2]}{(mB)^{1/3}} + d_1\frac{A_i'[(mB)^{2/3}\gamma^2]}{(mB)^{2/3}}\right\}, \tag{12a}$$

$$d_0 = \frac{\Gamma_0(\gamma) + \Gamma_0(-\gamma)}{2}, \qquad d_1 = \frac{\Gamma_0(\gamma) - \Gamma_0(-\gamma)}{2\gamma}, \tag{12b}$$

$$\Gamma_0(\zeta) = Q(\nu(\zeta))\,\frac{d\nu}{d\zeta}, \qquad \frac{d\nu}{d\zeta} = \frac{\gamma^2 - \zeta^2}{\Phi'(\nu(\zeta))}, \tag{12c}$$

where A_i and A_i' are the Airy function and its derivative, respectively, and d_0 and d_1 are coefficients in the asymptotic expansion. It is worth mentioning that, $\pm\gamma$ turn out to be the locations of the saddle points $\nu^{\pm}$ in the ζ-plane. The Airy function and its derivative provide a smooth transition from the subsonic portion of the blade to the supersonic portion. For $\gamma = 0$ (i.e., sonic sources) A_i and A_i' are $O(1)$ and, consequently, I_{n_p} is proportional to the inverse fractional 1/3-powers of mB. For $\gamma \neq 0$ (i.e., subsonic/supersonic sources), and large mB, A_i is $O((mB)^{-1/6})$ and A_i' is $O((mB)^{1/6})$ and, consequently, I_{n_p} is proportional to the inverse 1/2-power of mB as expected. Upon inserting for I_{n_p} in Eq. (9a) from Eq. (12a) and adding the contributions from all the N_p panels, the complex Fourier harmonic component, $p_{mB}(\mathbf{x})$, can be calculated.

At this point it should be pointed out that the analysis just described differs from that presented by Parry and Crighton [15] in that they use asymptotic forms of the Bessel functions in conjunction with the two-variable stationary phase method to asymptotically evaluate the surface integrals in Eq. (7). The key difference between the two analyses lies in their differing points of view. While, the approach described in Ref. [15] seeks to take advantage of the interference between the acoustic pressure disturbances arriving at the observer location emitted from the various sources distributed over the blade surface, the present method is built upon the idea that there is "self-interference" between the acoustic pressure signals emitted by the same source over one period of its revolution. From a practical stand point, the goal in Ref. [15] is to circumvent the time-consuming computations required in a full scale analysis by developing simple approximations to the noise field of a many-bladed propeller in order to gain insight into the importance of various physical parameters which influence the noise radiation characteristics of a propeller. The aim of the current approach is to provide an efficient way of carrying out a full scale analysis which, at the same time, is also amenable to systematic parametric studies of the sort envisioned in Ref. [15].

In order to assess the accuracy of the formula given by Eq. (12a), its predictions for a test problem were compared with those obtained through direct numerical integration of the θ integral in Eq. (9b). The test case chosen was an SR7 propfan operating in cruise conditions. An estimate for the aerodynamic loading distribution on the propfan blades, found by Nallasamy and Groeneweg [16] using an Euler CFD code developed by Whitfield et al. [17], was used along with the detailed geometric description

of the blade planform as input to the acoustic calculations. The results are summarized in Figs. (3) and (4).

In Fig.(3), sideline directivity of the BPF sound pressure level (SPL) is shown for two representative sets of observer locations; a near-field set and a far-field set. These correspond to two different sideline distances; one at $x_2 = 1.5R_{tip}$ and the other at $x_2 = 5R_{tip}$. In each case, the observer axial location was varied between $x_1 = -R_{tip}$ (i.e., forward of the plane of rotation) and $x_1 = +2R_{tip}$ (i.e., aft of the plane of rotation). The solid lines represent the asymptotic estimates of the SPLs, and the dotted lines their numerically computed values. As it can be seen, both in the near- and far-fields, the agreement between the numerical results and the asymptotic estimates is quite good, with the maximum error of about $1.5dB$ occurring at $0.5R_{tip}$ aft of the plane of rotation for the near-field observer.

Due to the nature of the asymptotic expansion, the maximum error in approximation occurs for the lowest value of the mB parameter, which is $m = 1$ corresponding to the BPF. As m increases, the error in the asymptotic approximations diminishes rapidly. Therefore, it is no surprise that the agreement between the estimates obtained from the asymptotic formula and the numerically computed results improves with increasing harmonic order. This result is highlighted in Fig. (4), where the waveforms of the radiated sound at the $0.5R_{tip}$ aft location for the two sideline distances mentioned earlier are presented. Note that, at the axial location chosen, the asymptotic estimate of the BPF sound pressure level deviated the most from their numerically computed values (see Fig. (3)). Once again, the agreement is exceptionally good, particularly at the far-field location where the asymptotic and numerical results are virtually indistinguishable from each other. In constructing the waveforms the first ten harmonics were used, which meant that, in carrying out the numerical integration, a progressively finer integration step size had to be utilized. This of course was reflected in an increase in the required computation time. The asymptotic estimates on the other hand, required virtually no additional time as compared with that required to compute the BPF results. This is simply due to the fact that the location of the saddle points and steepest descent paths, and the structure of the conformal map are independent of the parameter mB. It is worth mentioning that the amount of time required to construct the waveforms using the asymptotic method was more than an order of magnitude smaller than that required in the full numerical integration!

Having demonstrated the utility of present approach, we next outline the extension to include the angle of attack effect. Once again, for brevity, only important steps in the analysis are presented.

1.2.2 Non-Zero Angle of Attack Case ($\alpha \neq 0$)

In general, the development of the analysis in this case follows closely that presented in the previous section. However, the details of the analysis itself

are somewhat more complicated. For example, the phase function $\Phi(\theta, \alpha)$, (which is now more complicated than that for $\Phi(\theta, 0)$ given by Eq. (9c)), has four saddle points (i.e., $\Phi'(\nu, \alpha) = 0$ is a quartic equation). While, in principle, it is possible to find the roots of a quartic analytically, the expressions involved are rather lengthy. Fortunately, since in most practical applications of interest, the propeller angle of attack is small (typically no more than 5°), it is possible to find analytic approximations to the saddle points. This is done by treating the angle of attack case as a small perturbation to the zero angle of attack case (henceforth called the unperturbed case). The details of this development are given below where for convenience the analysis is carried out in terms of the parameter $M_{03} = M_0 \sin\alpha$, instead of α itself.

We begin by noting that for a small angle of attack, M_{03} is a small parameter, i.e., $|M_{03}| \ll 1$). Using perturbation analysis (see, for example, Bender and Orszag [18]) it can be shown that two of the four roots of $\Phi'(\nu, M_{03}) = 0$, denoted by $\hat{\nu}^{\pm}$, lie near those of the unperturbed problem $\Phi'(\nu, 0) = 0$ (i.e., $\nu^{\pm}$), while the other two scale with the inverse powers of M_{03} and, thus, lie much farther away. Therefore, since the perturbations in the integration contours are also small, the asymptotic behavior of I_{n_p} is controlled by the pair of saddle points $\hat{\nu}^{\pm}$. Of course, they could also merge to give rise to a second order saddle point as in the unperturbed case.

To find $\hat{\nu}^{\pm}$, first the phase function $\Phi(\nu, M_{03})$ is expanded in a Taylor series about $M_{03} = 0$ as follows;

$$\Phi(\nu, M_{03}) = \Phi_0(\nu) + M_{03}\Phi_1(\nu) + \frac{1}{2}M_{03}^2\Phi_2(\nu) + O(M_{03}^3), \qquad (13a)$$

where

$$\Phi_0(\nu) = \Phi(\nu, 0), \qquad \Phi_1(\nu) = \left[\frac{\partial\Phi(\nu, M_{03})}{\partial M_{03}}\right]_{M_{03}=0},$$

$$\Phi_2(\nu) = \left[\frac{\partial^2\Phi(\nu, M_{03})}{\partial M_{03}^2}\right]_{M_{03}=0}. \qquad (13b)$$

$\Phi_0(\nu)$ is given by Eq. (9c) (with θ replaced by ν), and $\Phi_1(\nu)$ and $\Phi_2(\nu)$ can be easily found by carrying out the differentiations with respect to M_{03}. Since, the salient features of the analysis which follows could be demonstrated without the need for the explicit expressions for $\Phi_1(\nu)$ and $\Phi_2(\nu)$, they are not given here in order to conserve space. The reason for retaining second order terms in Eq. (13a) will become clear shortly.

Next, Eq. (13a) is differentiated with respect to ν and set equal to zero;

$$\Phi'(\nu, M_{03}) \simeq \Phi_0'(\nu) + M_{03}\Phi_1'(\nu) + \frac{1}{2}M_{03}^2\Phi_2'(\nu) = 0, \qquad (14)$$

where the higher order terms in M_{03} are neglected to maintain consistency. Rewriting the resulting equation in terms of the auxiliary variable $\xi = \cos\nu$ and employing the notation used in Eq. (10), we find that,

$$(ab/2)^2\xi^2 - b\xi + 1 - (ab/2)^2 + 2M_{03}\left[(1-b\xi)\Phi_1'(\cos^{-1}\xi)\right] +$$

$$M_{03}^2(1-b\xi)\left[\Phi_1''(\cos^{-1}\xi) + \Phi_2'(\cos^{-1}\xi)\right] = 0, \qquad (15)$$

where, as before, only the second order terms are retained. Note that, when $M_{03} = 0$, Eq. (15) reduces to the unperturbed case given by Eq. (10). Therefore, as pointed out earlier, it is reasonable to expect that two of its roots lie near those of the unperturbed case. In order to solve Eq. (15) for the desired roots, $\hat{\xi}^{\pm} = \cos\hat{\nu}^{\pm}$, the functions inside the curly brackets are expanded in a Taylor series about the unperturbed roots $\xi^{\pm} = \cos\nu^{\pm}$. After collecting terms we find that Eq. (15) can be approximated by:

$$\left[(ab/2)^2 + M_{03}H_2^{\pm}\right]\xi^2 - \left[b - 2M_{03}(H_1^{\pm} + \xi^{\pm}H_2^{\pm})\right]\xi +$$

$$\left[1 - (ab/2)^2 + M_{03}(2H_0^{\pm} - 2\xi^{\pm}H_1^{\pm} + \xi^{\pm^2}H_2^{\pm}) + M_{03}^2K_0^{\pm}\right] = 0, \qquad (16a)$$

where

$$H_0^{\pm} = (1-b\xi^{\pm})\Phi_1'(\cos^{-1}\xi^{\pm}), \qquad (16b)$$

$$H_1^{\pm} = -\left[\frac{1-b\xi^{\pm}}{(1-\xi^{\pm^2})^{1/2}}\,\Phi_1''(\cos^{-1}\xi^{\pm}) + b\Phi_1'(\cos^{-1}\xi^{\pm})\right], \qquad (16c)$$

$$H_2^{\pm} = \left\{\frac{1-b\xi^{\pm}}{1-\xi^{\pm^2}}\,\Phi_1'''(\cos^{-1}\xi^{\pm}) - \right.$$

$$\left.\left[\frac{\xi^{\pm}(1-b\xi^{\pm})}{(1-\xi^{\pm^2})^{3/2}} - \frac{2b}{(1-\xi^{\pm^2})^{1/2}}\right]\Phi_1''(\cos^{-1}\xi^{\pm})\right\}, \qquad (16d)$$

$$K_0^{\pm} = (1-b\xi^{\pm})\left[\Phi_1''(\cos^{-1}\xi^{\pm}) + \Phi_2'(\cos^{-1}\xi^{\pm})\right]. \qquad (16e)$$

$H_0^{\pm}$, $H_1^{\pm}$, $H_2^{\pm}$ denote the coefficients of successive terms in the Taylor series expansion of the function inside the first curly bracket in Eq. (15), and $K_0^{\pm}$ denotes the leading term in the Taylor series expansion of the function inside the second curly bracket. Note that, $\cos^{-1}\xi^{\pm} = \nu^{\pm}$ in Eqs. (16a-16e).

The roots of this "new" quadratic can now be easily found. Since, Eq. (16a) has two roots for each of ξ^+ and ξ^-, we choose the root that reduces

to ξ^+ or ξ^- in the limit of $M_{03} \to 0$. As expected, $\hat{\xi}^\pm$ turn out to be only slightly different from the unperturbed roots $\xi^\pm$. It is worth mentioning that alternative perturbation methods could be used to find $\hat{\xi}^\pm$. However, the particular approach described above provides a uniform representation of the roots even when the unperturbed part of Eq. (16a) has a single double root (i.e., the sonic condition for the unperturbed problem). Near that condition the accuracy of the approximation drops to $O(M_{03}^{5/2})$. This is why in the original expansion (Eq. (13a)) the second order terms were retained. If only the first order terms were kept, near the sonic condition, the accuracy would be no more than $O(M_{03}^{1/2})$. With the two perturbed saddle points $\hat{\nu}^\pm$ now known, the asymptotic expansion of I_{n_p} can be carried out following the same procedure as was outlined in the previous section; the difference being that $\Phi(\nu, \alpha)$ is now replaced by the three terms on the right hand side of the Eq. (13a), and $\nu^\pm$ are replaced by $\hat{\nu}^\pm$.

Preliminary applications of the angle of attack formula to a few test cases have been rather encouraging. As in the case of zero angle of attack, it provides accurate estimates for the integral I_{n_p}. The utility of the method in solving realistic problems is demonstrated with the following example which involves the prediction of the spectrum of noise of SR7 propfan operating in cruise and at an angle of attack of $\alpha = 1.6°$. The unsteady aerodynamic loading distribution for this case was computed numerically by Nallasamy and Groeneweg [19] and was shown (see Heidelberg and Nallasamy [20]) to be in quite reasonable qualitative , as well as quantitative, agreement with the experimentally measured airloads. Using this aerodynamic loading distribution along with a detailed geometric description of the blade geometry as input, calculations for the spectrum of the noise of the propfan were carried out utilizing the asymptotic formula. The results were then corrected for non-free-field effects (such as scattering) which are not accounted for in the theoretical model. The corrections used, which were found in Spence [21], were $1.0, 3.6$ and $5.3dB$ for the first three harmonics, respectively. For higher harmonics a uniform correction of $5.0dB$ was assumed. The experimentally measured spectrum corresponding to this case was presented in Ref. [22], as part of the Propfan Test Assessment (PTA) program (see Poland et al. [23]). The comparison between the measured and asymptotically computed spectra is presented in Fig. (5). In general, the agreement is quite good with appreciable deviations occurring only at higher harmonics where the neglected quadrupole sources probably play an important role.

1.3 Concluding Remarks

An asymptotic approach was presented which allows for accurate and efficient calculation of the noise field of a propfan at angle of attack with-

out the need for simplifying assumptions usually employed in propeller noise theories. A closed form expression, involving the Airy function and its derivative, gives a uniform representation of the propeller noise field characteristics in both the near- and far-fields. The preliminary results shown here indicate that the method provides a useful theoretical tool in propeller noise research.

1.4 Acknowledgements

This work was supported under NASA grant NAS3-25266 and carried out at NASA Lewis Research Center in Cleveland, Ohio. The author wishes to thank Drs. Robert Rubinstein, Ambady Suresh and Paul Giel for many stimulating discussions. The help of Mrs. Tammy Langhals in typing and preparation of the manuscript is also gratefully acknowledged.

1.5 References

1. Woodward, R.P., "Measured Noise of a Scale Model High Speed Propeller at Simulated Takeoff/Approach Conditions," AIAA paper 87-0526, January 1987, also NASA-TM-88920.

2. Heidelberg, L.J. and Clark, B.J., "Preliminary Results of Unsteady Blade Surface Pressure Measurements for the SR-3 Propeller," AIAA paper 86-1893, July 1986, also NASA-TM-87352.

3. Nallasamy, M. and Groeneweg, J.F., "Unsteady Blade Surface Pressure on a Large-Scale Advanced Propeller: Prediction and Data," AIAA paper 90-2402, July 1990.

4. Hanson, D.B., "Unified Aeroacoustic Analysis for Highspeed Turboprop Aerodynamics and Noise. Vol. I: Development of Theory for Blade Loading, Wakes and Noise," NASA-CR-4329, to be published.

5. Mani, R., "The Radiation of Sound from a Propeller at Angle of Attack," NASA-CR-4264, January 1990.

6. Krejsa, E., "Prediction of the Noise from a Propeller at Angle of Attack," AIAA paper 90-5954, October 1990.

7. Ffowcs Williams, J.E. and Hawkings, D.L., "Sound Generation by Turbulence and Surfaces in Arbitrary Motion," Phil. Trans. R. Soc. Lond. Series A, Vol. 264, May 8, 1969, 321-342.

8. Hawkings, D.L. and Lowson, M.V., "Theory of Open Supersonic Rotor Noise," J. Sound Vib. 36(1), 1974, 1-20.

9. Hanson, D.B., "Near Field Frequency Domain Theory for Propeller Noise," AIAA J., Vol. 23, April 1985, 499-504.

10. Goldstein, M.E., AEROACOUSTICS, McGraw-Hill, New York, 1976, 189-192.

11. Farassat, F., "Linear Acoustic Formulae for Calculation of Rotating Blade Noise," AIAA J., Vol. 19, 1981 1122-1130.

12. Nallasamy, M., E. Envia, B.J. Clark, and J.F. Groeneweg, "Near-Field Noise of a Single Rotation Propfan at an Angle of Attack," AIAA paper 90-3953, also NASA-TM-103645, 1990.

13. Chester, C., B. Friedman and F. Ursell, "An Extension of the Method of Steepest Descent," Proc. Camb. Phil. Soc. 53, 1957, 599-611.

14. Bleistein, N. and R.A. Handelsman, ASYMPTOTIC EXPANSIONS OF INTEGRALS, Dover Publications Inc., New York, 1986, 369-374.

15. Parry A.B. and D.G. Crighton, "Asymptotic Theory of Propeller Noise-Part I: Subsonic Single-Rotation Propeller," AIAA J., Vol. 27(9), 1989, 1184-1190.

16. Nallasamy, M. and J.F. Groeneweg, "Prediction of Unsteady Blade Surface Pressures on an Advanced Propeller at an Angle of Attack," J. Aircraft, Vol. 27(9), September 1990, 789- 803.

17. Whitfield, D.L., T.W. Swafford, J.M. Janus, R.A. Mulac, and D.M. Belk, "Three Dimensional Unsteady Euler Solutions for Propfans and Counter Rotating Propfans," AIAA paper 87-1197, June 1987.

18. Bender, C.M. and S.A. Orszag, ADVANCED MATHEMATICAL METHODS FOR SCIENTISTS AND ENGINEERS, McGraw-Hill, New York, 1978, 319-330.

19. Nallasamy, M. and J.F. Groeneweg, "Unsteady Euler Analysis of the Flow Field of a Propfan at an Angle of Attack," AIAA paper 90-0339, October 1990.

20. Heidelberg, L.J. and M. Nallasamy, "Unsteady Blade Pressure Measurements for the SR-7A Propeller at Cruise Conditions," AIAA paper 90-4022, October 1990, also NASA-TM-103606.

21. Spence, P.L., "Progress Report on PTA Noise Prediction," April 5, 1990. 22. Lockheed/NASA-Lewis Propfan Test Assessment Program, Acoustic Flight Research Data, Yearly Status Review - Dec. 1987.

23. Poland, D.T., H.L. Bartel and P.C. Brown, "PTA Flight Test Review," AIAA paper 88-2803, July 1988.

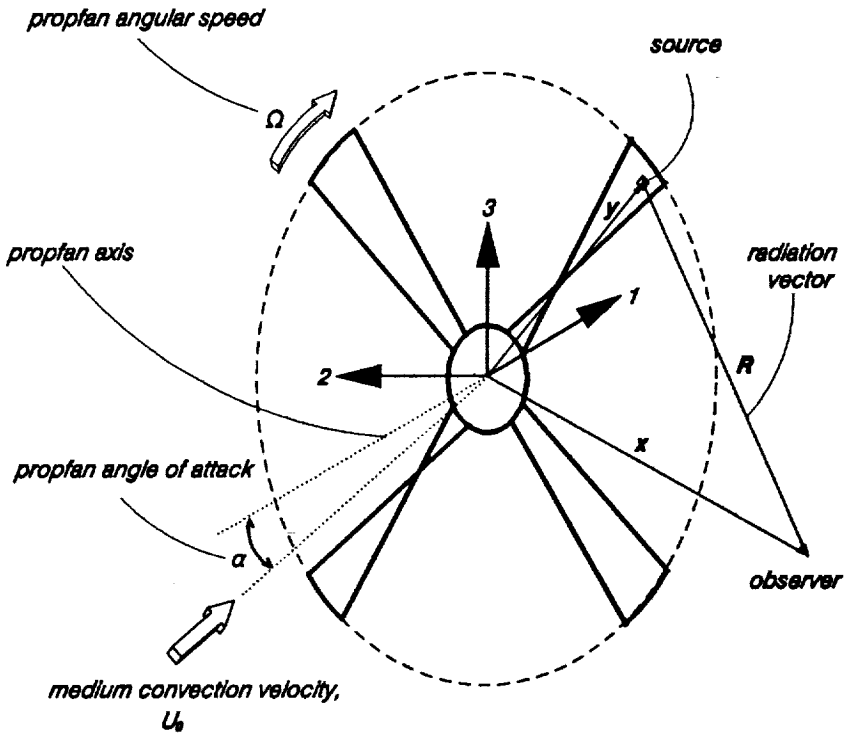

Fig. (1) Definitions of Geometry and Coordinate System.

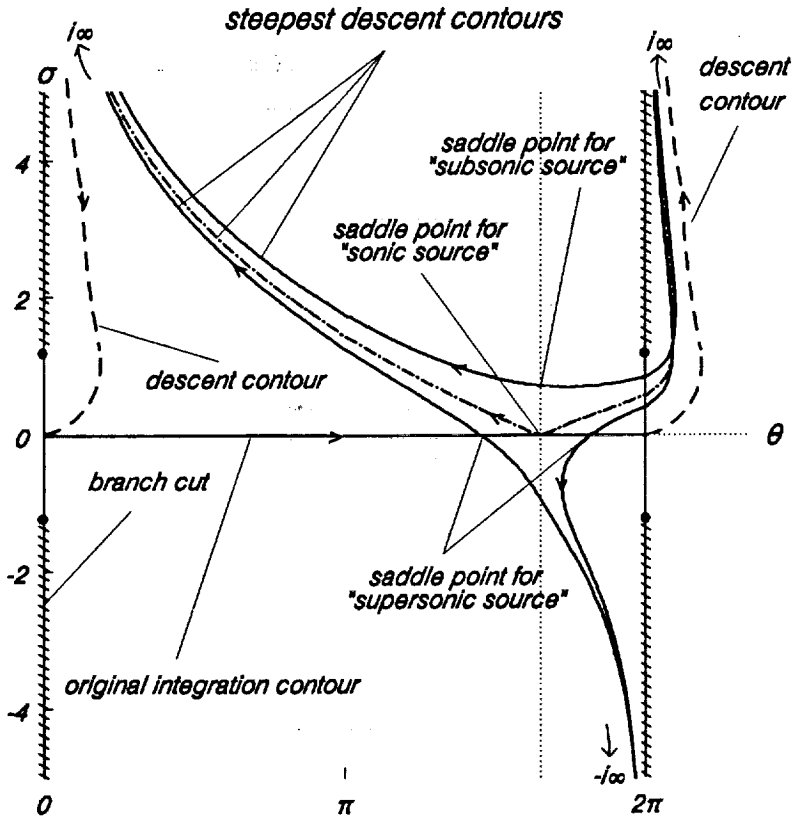

Fig. (2) Saddle Points and Steepest Descent Contours in the Complex ν-Plane.

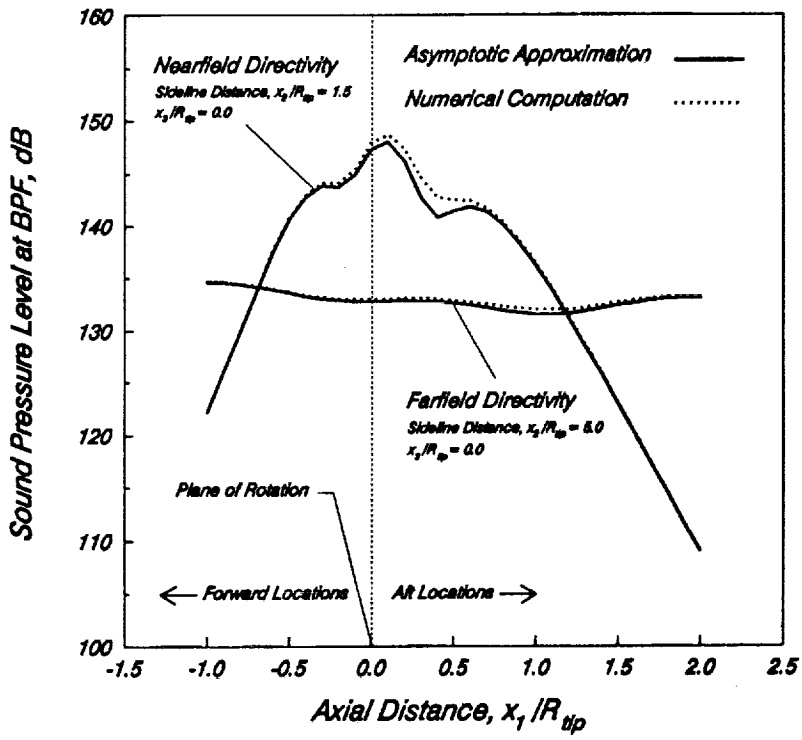

Fig. (3) Comparisons of Predicted Sideline Directivities of SR7 Propfan at Cruise Conditions and Zero Angle of Attack ($\alpha = 0$).

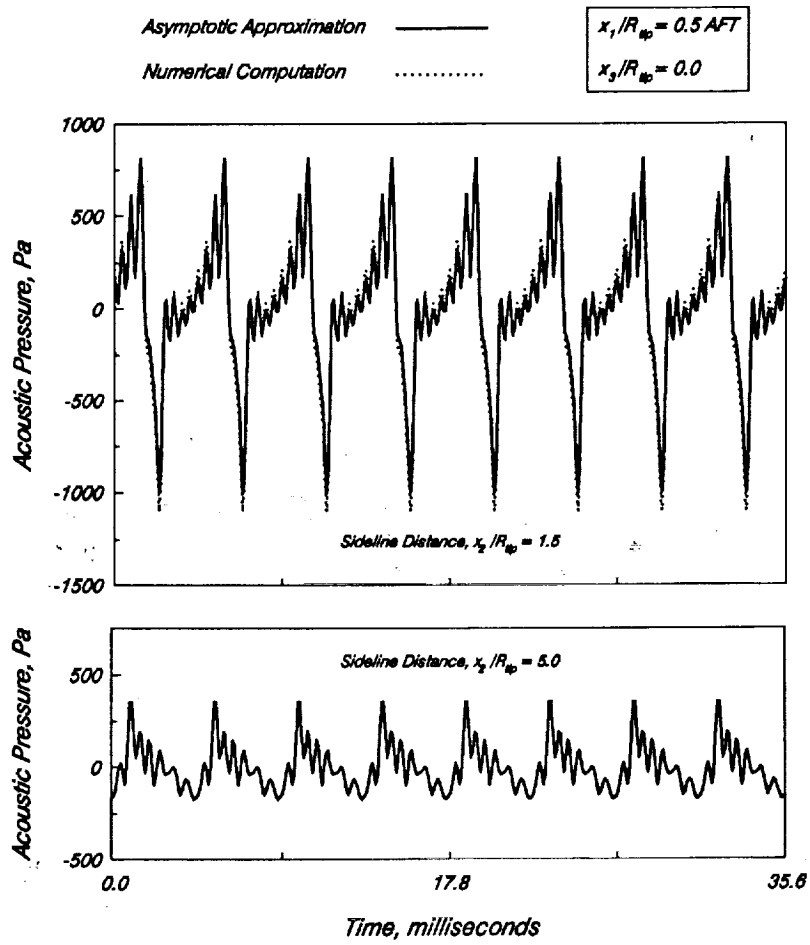

Fig. (4) Comparisons of Predicted Pressure Waveforms for SR7 Propfan at Cruise Conditions and Zero Angle of Attack ($\alpha = 0$).

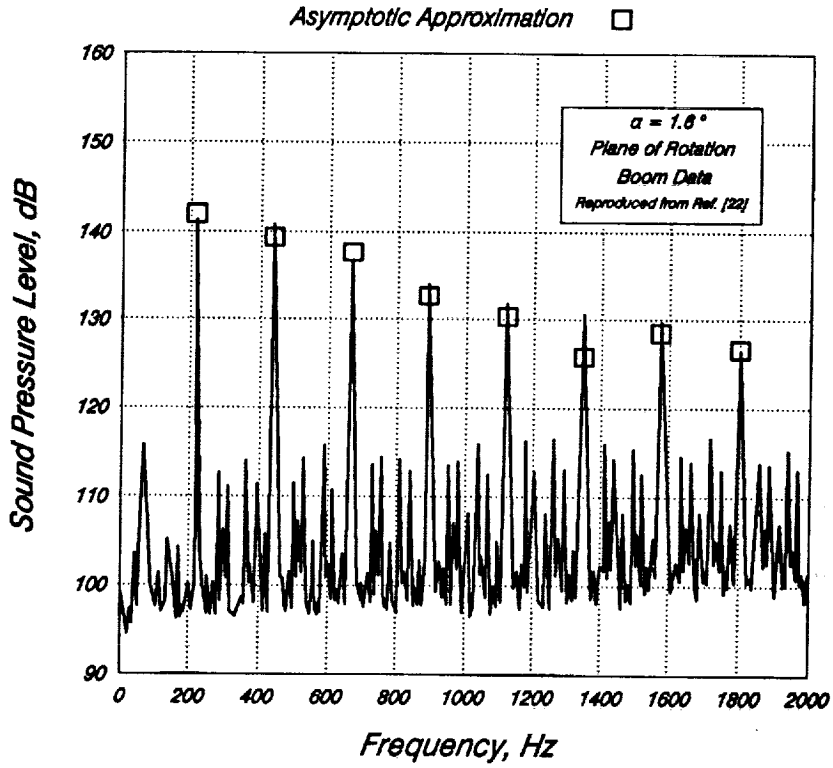

Fig. (5) Comparison of Measured and Predicted Pressure Spectra for SR7 Propfan at Cruise Conditions and Angle of Attack ($\alpha = 1.6°$). Spectra Presented for a Boom Lcation in the Plane of Rotation of Propfan (see Ref. [22] for details).

REPORT DOCUMENTATION PAGE

Form Approved
OMB No. 0704-0188

1. AGENCY USE ONLY (Leave blank)	2. REPORT DATE	3. REPORT TYPE AND DATES COVERED
	October 1991	Final Contractor Report

4. TITLE AND SUBTITLE

Prediction of Noise Field of a Propfan at Angle of Attack

5. FUNDING NUMBERS

WU-535-03-10
C-NAS3-25266

6. AUTHOR(S)

Edmane Envia

7. PERFORMING ORGANIZATION NAME(S) AND ADDRESS(ES)

Sverdrup Technology, Inc.
Lewis Research Center Group
2001 Aerospace Parkway
Brook Park, Ohio 44142

8. PERFORMING ORGANIZATION REPORT NUMBER

E-6645

9. SPONSORING/MONITORING AGENCY NAMES(S) AND ADDRESS(ES)

National Aeronautics and Space Administration
Lewis Research Center
Cleveland, Ohio 44135-3191

10. SPONSORING/MONITORING AGENCY REPORT NUMBER

NASA CR-189047

11. SUPPLEMENTARY NOTES

Project Manager, John F. Groeneweg, Propulsion Systems Division, NASA Lewis Research Center, (216) 433-3945. Prepared for the Sixth International Symposium on Unsteady Aerodynamics, Aeroacoustics, and Aeroelasticity of Turbomachines and Propellers sponsored by the International Union for Theoretical and Applied Mechanics, Notre Dame, Indiana, September 15-19, 1991.

12a. DISTRIBUTION/AVAILABILITY STATEMENT

Unclassified - Unlimited
Subject Category 71

12b. DISTRIBUTION CODE

13. ABSTRACT *(Maximum 200 words)*

A method for predicting the noise field of a propfan operating at angle of attack to the oncoming flow is presented. The method takes advantage of the high-blade-count of the advanced propeller designs to provide an accurate and efficient formula for predicting their noise field. The formula, which is written in terms of the Airy function and its derivative, provides a very attractive alternative to the use of numerical integration. A preliminary comparison shows rather favorable agreement between the predictions from the present method and the experimental data.

14. SUBJECT TERMS

Propeller noise; Angle of attack; Moving medium formulation; Uniform asymptotic expansion; Asymptotic formula; Perturbation method

15. NUMBER OF PAGES

22

16. PRICE CODE

A03

17. SECURITY CLASSIFICATION OF REPORT	18. SECURITY CLASSIFICATION OF THIS PAGE	19. SECURITY CLASSIFICATION OF ABSTRACT	20. LIMITATION OF ABSTRACT
Unclassified	Unclassified	Unclassified	